Published February 26, 2016

ORIGINAL RESEARCH

An Expanded Maize Gene Expression Atlas based on RNA Sequencing and its Use to Explore Root Development

Scott C. Stelpflug, Rajandeep S. Sekhon, Brieanne Vaillancourt, Candice N. Hirsch, C. Robin Buell, Natalia de Leon, and Shawn M. Kaeppler*

Abstract

Comprehensive and systematic transcriptome profiling provides valuable insight into biological and developmental processes that occur throughout the life cycle of a plant. We have enhanced our previously published microarray-based gene atlas of maize (*Zea mays* L.) inbred B73 to now include 79 distinct replicated samples that have been interrogated using RNA sequencing (RNA-seq). The current version of the atlas includes 50 original array-based gene atlas samples, a time-course of 12 stalk and leaf samples postflowering, and an additional set of 17 samples from the maize seedling and adult root system. The entire dataset contains 4.6 billion mapped reads, with an average of 20.5 million mapped reads per biological replicate, allowing for detection of genes with lower transcript abundance. As the new root samples represent key additions to the previously examined tissues, we highlight insights into the root transcriptome, which is represented by 28,894 (73.2%) annotated genes in maize. Additionally, we observed remarkable expression differences across both the longitudinal (four zones) and radial gradients (cortical parenchyma and stele) of the primary root supported by fourfold differential expression of 9353 and 4728 genes, respectively. Among the latter were 1110 genes that encode transcription factors, some of which are orthologs of previously characterized transcription factors known to regulate root development in *Arabidopsis thaliana* (L.) Heynh., while most are novel, and represent attractive targets for reverse genetics approaches to determine their roles in this important organ. This comprehensive transcriptome dataset is a powerful tool toward understanding maize development, physiology, and phenotypic diversity.

Published in The Plant Genome 9
doi: 10.3835/plantgenome2015.04.0025

© Crop Science Society of America
5585 Guilford Rd., Madison, WI 53711 USA
This is an open access article distributed under the CC BY-NC-ND license (http://creativecommons.org/licenses/by-nc-nd/4.0/).

MAIZE is a crop of worldwide importance and a valuable model for crop biological research. Substantial research on maize has focused on characterization of the relationships between aerial phenotypes and the underlying molecular networks. However, elucidation of the molecular mechanisms governing maize root growth and development remains comparatively underdeveloped. Indeed, it has been proposed that belowground characteristics of plants, such as root system architecture, nutrient uptake, and N fixation, are promising features to be improved on to enable a second "Green Revolution" (Lynch, 1995).

Comprehensive knowledge of the transcriptome is an integral component of systems biology, a holistic approach that strives to understand the role and interaction of individual biological components in shaping phenotypes. Global transcriptome profiling provides a mechanism to access gene networks for the discovery of functional connections between genes, messenger RNAs (mRNAs; and their regulatory proteins), and temporal and spatial

S.C. Stelpflug, N. de Leon, and S.M. Kaeppler, Dep. of Agronomy, Univ. of Wisconsin–Madison, Madison, WI 53706; R.S. Sekhon, Dep. of Genetics and Biochemistry, Clemson Univ., Clemson, SC; B, Vaillancourt and C.R. Buell, Dep. of Plant Biology, Michigan State Univ., East Lansing, MI; and DOE Great Lakes Bioenergy Research Center, East Lansing, MI; C.N. Hirsch, Dep. of Agronomy and Plant Genetics, Univ. of Minnesota, St. Paul, MN; N. de Leon and S.M. Kaeppler, DOE Great Lakes Bioenergy Research Center, Madison, WI; S.C. Stelpflug and R.S. Sekhon contributed equally to this work. Sequences are available in the Sequence Read Archive at the National Center for Biotechnology Information (accession numbers PRJNA171684 and SRP010680). Received 21 Apr. 2015. Accepted 28 July 2015. *Corresponding author (smkaeppl@wisc.edu).

Abbreviations: CP, cortical parenchyma; DAP, days after pollination; DAS, days after sowing; FPKM, fragments per kb exon model per million mapped fragments; GO, gene ontology; mRNA, messenger RNA; nt, nucleotide; PCA, principal component analysis; RNA-seq, RNA sequencing; ROS, reactive oxygen species; TF, transcription factor.

determination of complex traits through coordinated and dynamic gene networks (Komili and Silver, 2008). In plants, transcriptome profiles capturing development have been documented in several species including *A. thaliana* (Schmid et al., 2005), maize (Sekhon et al., 2011, 2013), rice (*Oryza sativa* L.) (Jiao et al., 2009), soybean [*Glycine max* (L.) Merr.] (Libault et al., 2010), barley (*Hordeum vulgare* L.) (Druka et al., 2006), Medicago (*Medicago truncatula* Gaertn.) (Benedito et al., 2008), *Lotus japonicus* (Regel) K. Larsen (Verdier et al., 2013), and Sorghum [*Sorghum bicolor* (L.) Moench] (Shakoor et al., 2014).

Transcriptome analysis efforts in maize have been enabled by access to a reference genome assembly (Schnable et al., 2009). We previously used maize genome sequences to design a custom NimbleGen array and developed a gene atlas to document transcription in 60 unique spatially and temporally separated tissues from 11 maize organs (Sekhon et al., 2011). This work characterized the global transcriptome of maize and found that a large amount of genes are expressed in all tissues (~45%), while a small but significant proportion (2.7%) exhibit organ specific expression patterns; the utility of this dataset was highlighted by examining gene expression and organ specification of lignin biosynthesis genes in maize (Sekhon et al., 2011).

Microarrays have subsequently been replaced by RNA-seq, which relies on sequencing-by-synthesis of complementary DNA fragments (Wang et al., 2009). RNA sequencing offers several advantages including lack of background noise commonly observed in microarrays as a result of cross-hybridization (Okoniewski and Miller, 2006, Royce et al., 2007), enhanced ability to detect alternative splicing (Mortazavi et al., 2008; Sultan et al., 2008), a large dynamic range (>9000-fold) of expression estimation, and an ability to discern expression of highly similar paralogs (Mortazavi et al., 2008; Wang et al., 2009; Grabherr et al., 2011). Subsequent to the original microarray study, we reported the transcriptome of a subset (18) of these 60 tissues using RNA-seq with varying read lengths (35, 76, or 101 nucleotide [nt]) and sequencing depths (5–28 million reads per biological replicate) (Sekhon et al., 2013). This dataset provided enhanced coverage of the transcriptome, with 82.1% of the filtered maize genes detected as expressed in at least one tissue by RNA-seq compared with only 56.5% detected by microarrays. Additionally, RNA-seq provided higher resolution for identifying tissue-specific expression as well as for distinguishing the expression profiles of closely related paralogs as compared with microarray-derived profiles (Sekhon et al., 2013). Other RNA-seq expression datasets in maize have focused on specific organs such as leaves, embryo, endosperm, and reproductive tissues (Li et al., 2010, 2014; Davidson et al., 2011; Chen et al., 2014).

Here, we report an expanded RNA-seq-based B73 gene atlas, encompassing 79 total RNA samples including 50 of the 60 tissues reported in the original microarray-based gene atlas (Sekhon et al., 2011), 12 additional postflowering stalk and leaf tissues that were previously profiled using microarrays (Sekhon et al., 2012), and 17 newly profiled root tissues. This comprehensive set of transcriptome profiles was produced with a single sequencing platform, uniform read length, and analyzed using a defined informatics pipeline and provides a new robust resource for gene discovery and gene validation in maize and other plant species.

MATERIALS AND METHODS

Plant Materials, Growing Conditions, and RNA Extraction

Maize inbred B73 was used for constructing all tissues of the expanded gene atlas. A concise description of the tissues collected to create the gene atlas is presented in Table 1. Images of selected tissues from the microarray-based atlas (Sekhon et al., 2011) are depicted in Supplemental Fig. S1a,b. Images of selected tissues from aging leaf and internode from Sekhon et al. (2012) are also depicted in Supplemental Fig. S1c. Manual separation of root cortical parenchyma and stele tissues was performed according to Saleem et al. (2010). Newly profiled root tissues are shown in Fig. 1 with nomenclature of adult root nodes described in Supplemental Fig. S2. Plants harvested for tissue were grown in growth chambers, greenhouse, or in the field (Table 1). For plants in growth chambers, seeds were surface sterilized for 5 min in a 1:1 solution of deionized H_20 and 6% NaClO followed by two washes with deionized H_20 for 1 min. Three seeds were placed between two sheets of brown germination paper (Anchor Paper) with an even horizontal space among them and starting one inch from the top of the sheet. Approximately 75 of such sandwich blots were placed in a container, soaked vertically in a plastic reservoir (47.5 [length] by 35 [width] by 25 cm [height]) filled with 5 L of nutrient solution consisting of NO_3 (7000 μM), P (250 μM), K (3000 μM), NH4 (1000 μM), Ca (2000 μM), SO_4 (500 μM), Mg (500 μM), Cl (25 μM), B (12.5 μM), Mn (1 μM), Zn (1 μM), Cu (0.25 μM), Mo (0.25 μM), and EDTA-Fe (25 μM). Seedlings were germinated and grown in a growth chamber in the Biotron, at the University of Wisconsin–Madison at 28 and 24°C (light vs. dark) under a 14:10 h (light/dark) regime with photosynthetically active radiation of 200 L mol photons m^{-2} s^{-1}. The relative humidity was maintained at 65%. The nutrient solution pH was daily adjusted to 6.0 with 1 M KOH and 1 M HCl. Plants were grown in the greenhouse or field as described earlier (Sekhon et al., 2011).

The number of plants per biological replicate varied depending on tissue type (Table 1). For embryonic and early postembryonic stages of root development, biological replicates were constituted of pooled samples from randomly chosen, healthy plants. The harvested tissues were immediately frozen in liquid nitrogen and stored at −80°C.

Table 1. Maize tissues of inbred B73 included in the RNA-seq gene expression atlas.

Organ group[†]	Tissue description[‡]	Growth stage at collection[§]	Growth method[¶]	Tissue designation	No. of plants per bioreplicate
Root	Primary root	3 DAS	GPNS	Primary_Root_3DAS	20
	Differentiation zone of primary root	3 DAS	GPNS	Root_DZ_3DAS	20
	Meristematic and elongation zones of primary root	3 DAS	GPNS	Root_MZ_and_EZ_3DAS	30
	Root stele	3 DAS	GPNS	Root_Stele_3DAS	30
	Root cortical parenchyma (CP)	3 DAS	GPNS	Root_CP_3DAS	30
	Primary root (GH)	6 DAS	GH	Primary_Root_GH_6DAS	3
	Root system	7 DAS	GPNS	Root_System_7DAS	3
	Primary root	7 DAS	GPNS	Primary_Root_7DAS	3
	Seminal roots	7DAS	GPNS	Seminal_Roots_7DAS	3
	Primary root zone 1	7 DAS	GPNS	Primary_Root_Z1_7DAS	30
	Primary root zone 2	7 DAS	GPNS	Primary_Root_Z2_7DAS	20
	Primary root zone 3	7 DAS	GPNS	Primary_Root_Z3_7DAS	10
	Primary root zone 4	7 DAS	GPNS	Primary_Root_Z4_7DAS	10
	Crown roots nodes 1–3	V7	GH	Crown_Roots_Nodes1–3_V7	2
	Crown roots node 4	V7	GH	Crown_Roots_Node4_V7	2
	Crown roots node 5	V7	GH	Crown_Roots_Node5_V7	2
	Crown roots node 5	V13	GH	Crown_Roots_Node5_V13	2
	Brace roots node 6	V13	GH	Brace_Roots_Node6_V13	2
Leaf	Coleoptile	6 DAS	GH	Coleoptile_GH_6DAS	
	Pooled leaves	V1	Field	Pooled_Leaves_V1	2–3
	Topmost leaf	V3	Field	Topmost_Leaf_V3	2–3
	Shoot tip	V5	Field	Shoot_Tip_V5	2–3
	Tip of stage 2 transition leaf	V5	Field	Tip_Stage2_Leaf_V5	2–3
	Base of stage 2 transition leaf	V5	Field	Base_Stage2_Leaf_V5	2–3
	Tip of stage 2 transition leaf	V7	Field	Tip_Stage2_Leaf_V7	2–3
	Base of stage 2 transition leaf	V7	Field	Base_Stage2_Leaf_V7	2–3
	Immature leaves	V9	Field	Immature_Leaves_V9	2–3
	Eighth leaf	V9	Field	Eighth_Leaf_V9	2–3
	Eleventh leaf	V9	Field	Eleventh_Leaf_V9	2–3
	Thirteenth leaf	V9	Field	Thirteenth_Leaf_V9	2–3
	Thirteenth leaf	VT	Field	Thirteenth_Leaf_VT	2–3
	Thirteenth leaf	R2	Field	Thrteenth_Leaf_R2	2–3
	Aging leaf	0–30 DAP1 (six tissues)	Field	Leaf_XDAP (X = number)	2–3
SAM and young stem	Stem and SAM	V1	Field	Stem_and_SAM_V1	2–3
	Stem and SAM	V3	Field	Stem_and_SAM_V3	2–3
Internode	First elongated internode	V5	Field	First_Internode_V5	2–3
	Fourth elongated internode	V9	Field	Fourth_Internode_V9	2–3
	Aging internode	0–30 DAP1 (six tissues)	Field	Internode_XDAP (X = number)	2–3
Reproductive	Immature tassel	V13	Field	Immature_Tassel_V13	2–3
	Meiotic tassel	V18	Field	Meiotic_Tassel_V18	2–3
	Anthers	R1	Field	Anthers_R1	2–3
	Immature cob	V18	Field	Immature_Cob_V18	2–3
	Prepollination cob	R1	Field	Pre-pollination_Cob_R1	2–3
	Silks	R1	Field	Silks_R1	2–3
Seed	*Whole seed*	2–24 DAP2 (12 tissues)	Field	Whole_Seed_XDAP (X = number)	2–3
	Endosperm	12–24 DAP (7 tissues)	Field	Endosperm_XDAP (X = number)	2–3
	Embryo	16–24 DAP (5 tissues)	Field	Embryo_XDAP (X = number)	2–3
	Pericarp	18 DAP	Field	Pericarp_18DAP	2–3

[†] SAM, shoot apical meristem.

[‡] Tissue description in bold type indicates an updated RNA-seq sample of original microarray tissue (Sekhon et al., 2011); Tissue description in bold italic indicates original microarray tissue and RNA-seq sample previously published in PLoS One study (Sekhon et al., 2013); Tissue descriptions in italic (no bold) indicate RNA-seq sample previously published in Plant Physiology study (Sekhon et al., 2012).

[§] DAS, days after sowing; V*n*, vegetative stage corresponding to the number of emerged leaves; VT, vegetative tasseling (last branch of tassel fully emerged; DAP, days after pollination; R1, reproductive 1; R2, reproductive 2; DAP1, samples collected every 6 d; DAP2, samples collected every other day.

[¶] GPNS, germination paper in nutrient solution; GH, greenhouse.

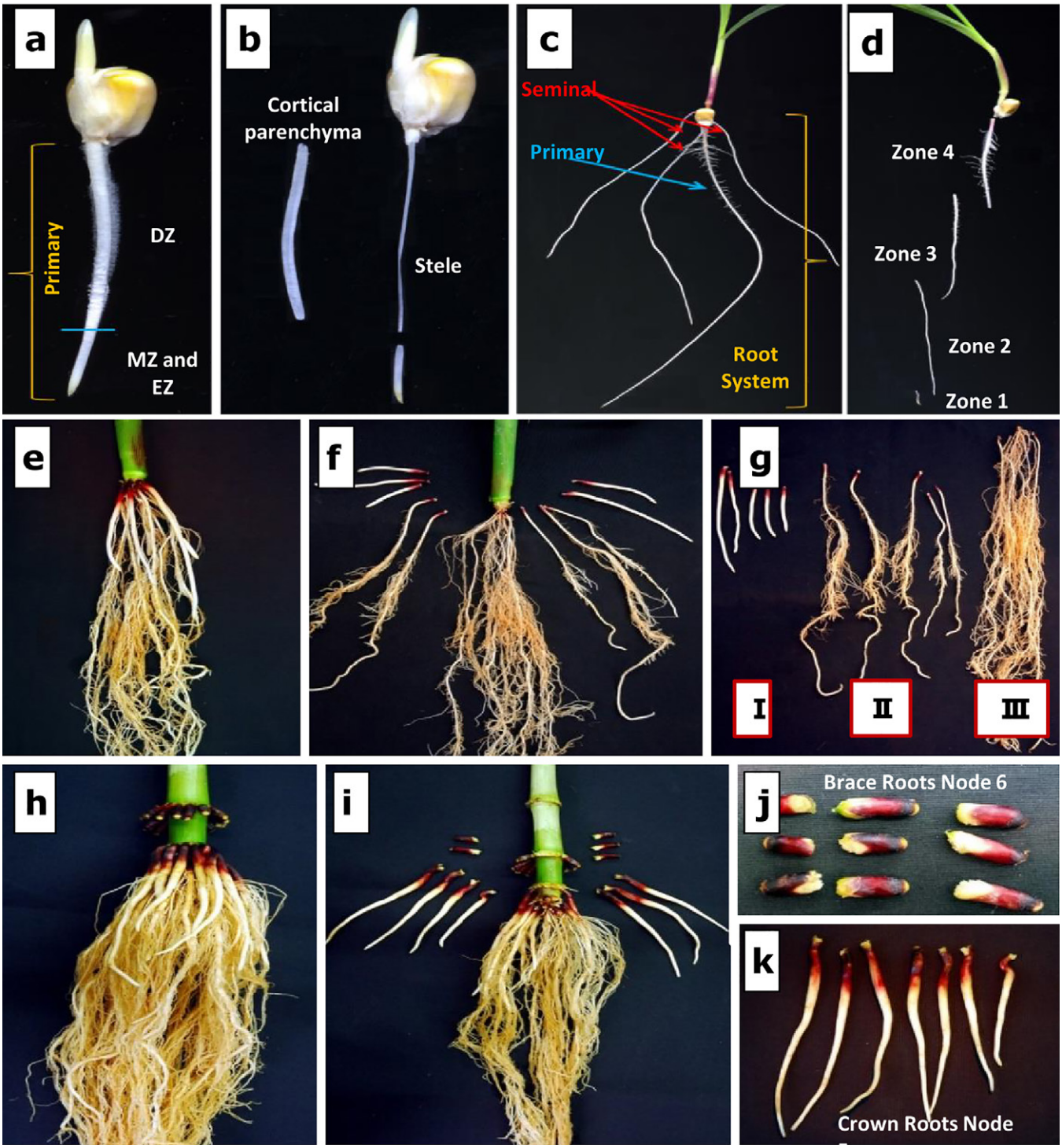

Figure 1. Embryonic and postembryonic root tissues included in the expanded RNA-seq gene atlas. (a) Primary root 3 d after sowing (3DAS). DZ, root differentiation zone; MZ, root meristematic zone; EZ, root elongation zones. (b) Root cortical parenchyma and stele of the differentiation zone 3DAS. (c) Root system (inclusive of primary and seminal roots) 7 d after sowing (7DAS). (d) Primary root. Z1, Zone 1 (first cm of root tip); Z2, Zone 2 (from end of Z1 to the point of root hair or lateral root initiation); Z3, Zone 3 (lower half of differentiation zone); Z4, Zone 4 (upper half of differentiation zone). (e) Whole postembryonic root system at developmental stage vegetative 7 (V7). (f) Dissection method of V7 root system. (g) Pooled tissue sampled for experiment: (I) crown roots Node 5, (II) crown roots Node 4, and (III) crown roots Nodes 1 through 3. (h) Whole postembryonic root system at V13. (i) Dissection of root system at developmental stage V13. (j) Pooled tissue from brace roots Node 6 (aboveground) sampled for experiment. (k) Pooled tissue from crown roots Node 5 sampled for experiment. Nomenclature of root nodes is described in Supplemental Fig. S2.

RNA Library Construction and Illumina Sequencing

RNA extraction, sample preparation, and sequencing were performed as described previously (Sekhon et al., 2013). Each library was sequenced, often multiple times and pooled, to obtain an average of ~25.3 million 100- to 101-nt single-end or paired-end raw reads (Supplemental Table S1). Sequence reads for each sample were mapped to v2 of the B73 reference genome assembly (http://ftp.maizesequence.org/release-5b/assembly/) (Schnable et al., 2009) using the same methods as previously described (Sekhon et al., 2013).

Principal Component Analysis and Hierarchical and K-Means Clustering

To facilitate graphical interpretation of relatedness among the 79 diverse tissues included in the expanded maize gene atlas, we reduced the dimensional expression data to two dimensions by principal component analysis (PCA) using the prcomp function in R software with default settings (R Core Development Team, 2014). The transformed and normalized gene expression values with $\log_2$ (fragments per kilobase [kb] exon model per million mapped fragments [FPKM] + 1) were used for the analysis of PCA, using only genes with an FPKM > 1 in at least one tissue. Hierarchical clustering of these same 79 tissues was based on the Pearson's correlations of the same transformed expression values. For the analysis of differentially expressed transcription factors, hierarchical clustering was performed by the hclust function in R software based on Euclidean distance with genes normalized via log2 transformation (R Core Development Team, 2014). K-means clusters were derived via log2 transformed FPKM values of 9347 differentially expressed genes (fourfold cut-off) from all pairwise comparisons of longitudinal zones as input. Analysis was performed using the K-means clustering module embedded in the MeV program (http://www.tm4.org/mev.html) using six clusters and 50 iterations. Six major clusters were chosen because partitioning the dataset into additional clusters did not reveal enrichment of additional biological gene ontology (GO) terms.

Differential Expression and Gene Ontology Enrichment Analysis

For any comparison between tissues, genes were considered differentially expressed if they varied by a conservative fourfold change in expression or more. Plant Gene Set Enrichment Analysis (PlantGSEA) was used to examine the biological functions of genes exhibiting fourfold change in expression for two separate biological comparisons: (i) cortical parenchyma (CP) vs. stele, and (ii) for genes in common K-means coexpression clusters across four longitudinal zones of the primary root (Yi et al., 2013). This tool examines overrepresentations among GO terms describing gene product species in three independent categories: biological process, molecular function, and cellular components (http://www.geneontology.org). This tool can also examine enrichments among specific gene families and other curated gene sets. To identify significantly overrepresented (false discovery rate < 5%) functional categories, a singular enrichment analysis via Fisher's exact test was performed using all genes in v2 of the maize B73 genome (n = 39,456) as the background gene set. Single enrichment analysis compares each annotated protein class with all annotated expressed proteins in a tissue. For nonexpressed genes in the gene atlas, GO enrichment analysis was performed with AgriGO (Du et al., 2010) via Fisher's exact test, using Yekutieli false discovery rate (Benjamini and Yekutieli, 2001) to correct for multiple testing with significance was determined as $P < 0.05$.

Comparative Genomics of Maize Candidate Genes

For the analysis of maize candidate transcription factor (TF) genes exhibiting enhanced spatiotemporal expression patterns within the maize root, we identified *Arabidopsis* orthologs using the Putative Orthologous Groups 2.0 (POGs) database (http://pogs.uoregon.edu/) (Tomcal et al., 2013). The POGs 2.0 relational database is designed to facilitate cross-species inferences about gene functions and gene models in plants by integrating data from rice, maize), *A. thaliana*, and poplar (*Populus trichocarpa* Torr. & A. Gray). The POGs 2.0 database places the complete predicted proteomes into POGs based on a mutual-best-hits strategy, with POG assignments subsequently evaluated by phylogenetic analysis (Walker et al., 2007). We selected the *Arabidopsis* ortholog with the highest percentage identity to the corresponding maize gene for our comparative genomics analysis of TF genes.

RESULTS AND DISCUSSION

Overview of Samples and Quality Assessment

We used RNA-seq to profile the transcriptome of 79 tissues, including 61 aboveground and 18 root tissues, representing distinct stages of maize plant development. These include 50 samples previously examined with microarrays (Sekhon et al., 2011) (Supplemental Fig. S1a,b), a time-course of 12 stalk and leaf samples spanning the flowering and grain-fill period described in an earlier study that used microarrays (Sekhon et al., 2012; Supplemental Fig. S1c), and a newly profiled set of 17 samples from the root system of seedling and adult plants (Fig. 1; Table 1). Most samples from previous studies were resequenced to enhance coverage and processed using the same analysis pipeline to generate the expression data in a uniform manner (Supplemental Table S1). For each sample, two or three biological replicates were examined and each biological replicate consisted of pooled tissue from 2 to 30 individual plants (Table 1; Supplemental Table S1). For each biological replicate, we generated an average of 25.3 million raw 100- to 101-nt

reads (Supplemental Table S1). Of these, across samples, 57.8 to 91.1% of the reads could be mapped (unique and multiple) to the B73 reference genome (AGPv2; Table S1) and were used for calculation of expression values measured in FPKM values. Since multiple transcripts arising from potential alternative splicing events have been predicted for the majority of maize genes, FPKM values were computed for every individual gene (Supplemental Dataset S1, S2) and on a per-transcript basis (Supplemental Dataset S3, S4). The biological replicates were highly correlated with an average Pearson's correlation coefficient of 0.982 ± 0.038 with 96.25% (197) of the correlations values (207 total) over 0.950 (Supplemental Table S2). Only two tissues (Endosperm_14DAP and Brace Root Node 6_V13) had more than one correlation value less than 0.950. For both of these tissues, it was bioreplicate two that contributed to the lower correlation values. Overall, these observations affirmed the reproducibility and quality of the biological replicates using RNA-seq.

Global Gene Expression Trends

To exclude genes with low confidence expression values, only those genes with an FPKM value >1 in at least one tissue were designated as expressed. Based on this criterion, 32,721 (82.9%) of the annotated genes were expressed in at least one tissue, indicating substantially higher representation of the transcriptome relative to the 56.5% of expressed genes captured in the previous array-based gene atlas (Sekhon et al., 2011). Diversity of transcriptional activity was highly variable across tissues, with the primary root 7 d after sowing (DAS) tissue expressing the largest number of genes (26,488; 67.1% of all genes), and the endosperm 24 d after pollination (DAP) tissue expressing the smallest number of genes (18,565; 47.3%) (Supplemental Fig. S3). Of the 6735 genes not expressed in any tissue, 62.4% are annotated as hypothetical or unknown according to the B73 reference gene annotation (version 5b). While some of these annotations may be artifacts, it is possible a subset of transcripts were not captured in our 79 tissue atlas survey as a result of very low transcript levels not captured by the current sequencing depth or lack of expression in the tissues sampled. Indeed, in a comparison of transcript abundance between shallow and an ultra-deep RNA-seq datasets derived from B73 seedling tissue, genes encoding TFs and regulators, often lowly transcribed, were not detected during shallow sampling (Martin et al., 2014). Furthermore, GO enrichment analysis showed that, of the nonexpressed genes with functional annotations (n = 1570), the three most overrepresented classes are response to external stimulus (GO: 0009605), gene expression (GO: 0010467), and transcription (GO: 0006350) (Supplemental Table S3). As we did not deliberately sample tissues exposed to any abiotic or biotic stressed tissues, this observation suggests that expansion of the atlas to include stressed tissues may provide a broader representation of the full B73 transcriptome. Regardless, the current 79-sample RNA-seq atlas provides a robust assessment of gene expression across a wide developmental series of maize that can be used for understanding key genes and genetic regulatory mechanisms involved in development as highlighted below.

The biological identity of tissues was well reflected in their respective transcriptomes as revealed by hierarchical clustering of Pearson's correlations and by PCA of all 79 tissues (Fig. 2; Supplemental Fig. S4). Most tissues clustered together based on their morphological, physiological, and developmental attributes and provided an interesting glimpse into the differentiation of plant organs. Additionally, less obvious degrees of biological relatedness were evident from clustering analysis. For instance, broad clustering of tissues containing meristems such as coleoptile, young stem and shoot apical meristems, base of leaf, developing inflorescences, and root tip tissues containing the meristematic zones (Brace Roots Node 6, Meristematic Zone [MZ] and Elongation Zone [EZ] Root 3DAS, and Primary Root Zone 1 7DAS), indicate shared transcriptional patterns resulting from meristem maintenance-related processes in these spatially distinct tissues. Similarly, both immature male (tassel) and female (cob) reproductive organs clustered fairly close together, consistent with their shared genetic underpinnings and morphological origins (Thompson and Hake, 2009; Vollbrecht and Schmidt, 2009; Brown et al., 2011; Eveland et al., 2014) and a previous study of the maize reproductive transcriptome (Davidson et al., 2011). However, specialized floral organs, such as the silks and anthers, have quite diverged functions, as evident from their fairly unique clustering pattern.

Because the newly profiled root tissues represent a significant addition to our previously published gene atlas and are a relatively less understood organ, we examined the root transcriptome in greater depth for insights related to development. Relative to the aboveground organs, root tissues shared similar global transcriptional patterns as indicated by their compact clustering via PCA (Supplemental Fig. S4). Despite global similarities, subtle but important differences among root tissues were evident from PCA involving only the 18 root tissues (Fig. 3). The first principle component (31.3% variance explained) separated samples primarily according to differentiation, with undifferentiated root meristems formed a distinct cluster compared with the differentiated tissues containing lateral roots and root hairs. This is clearly illustrated with the longitudinal dissection of the primary root into four zones, which all diverge related to the axis of PC1 according to their spatial designation along the primary root, with Zones 2 and 3 (the transition zones) close in proximity, indicating key spatial differences across the longitudinal axis. The second principle component (15.6% variance explained) separated root samples according to developmental stage, with the early stages of embryonic root development (3, 6, and 7 DAS tissues) grouping toward the positive spectrum of PC1, increasing with age to the

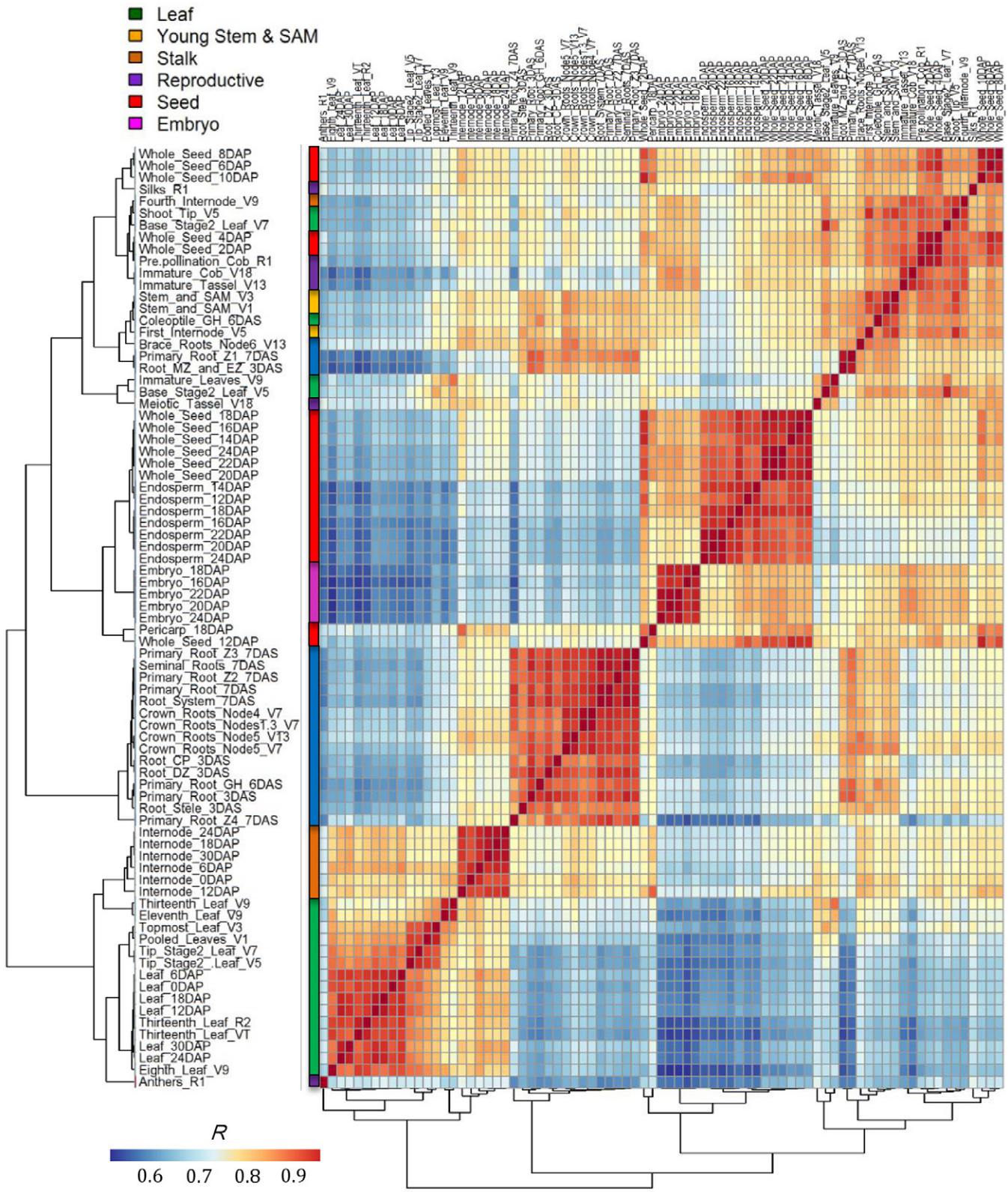

Figure 2. Global gene expression patterns reflect biological relatedness among maize tissues. Heat map of hierarchical clustering results of Pearson's correlations (*R*) for all 79 tissues included in the expanded atlas. Genes with a fragments per kb exon model per million mapped fragments (FPKM) > 1 in at least one tissue were log2, +1 transformed before analysis. The color scale indicates the degree of correlation. Samples were clustered based on their pairwise correlations.

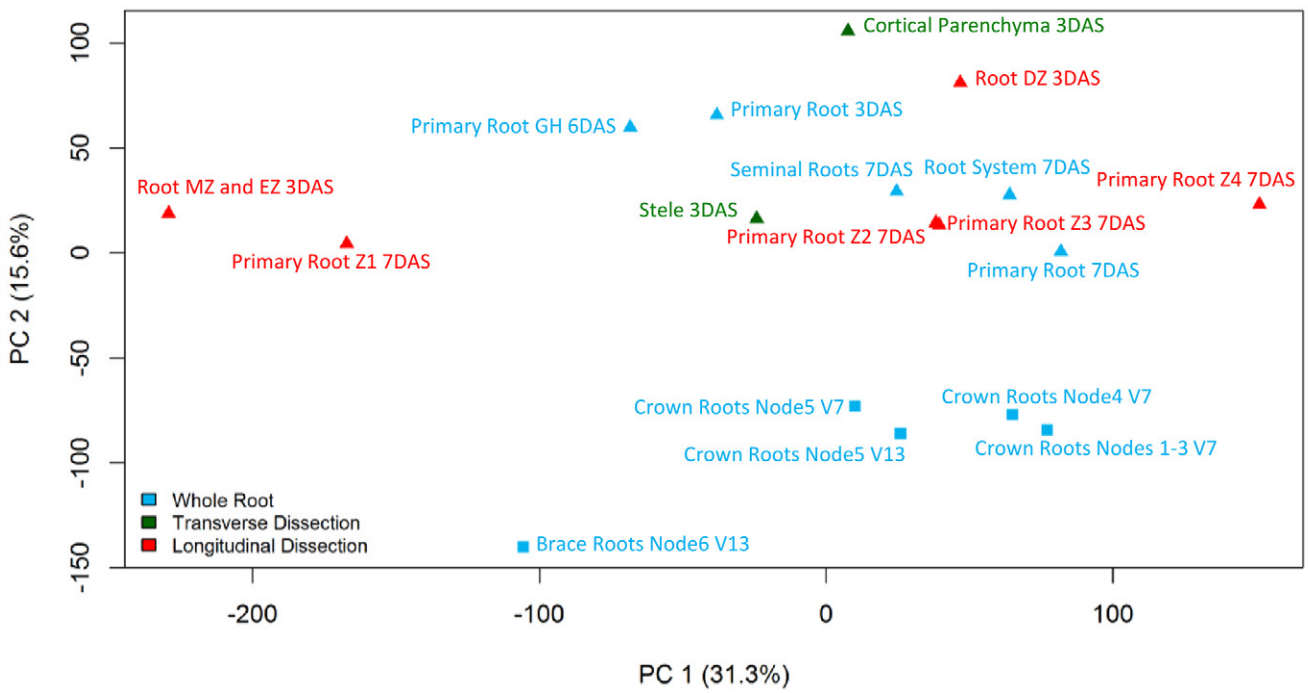

Figure 3. Principal component analysis (PCA) depicts relationships among maize root tissues. PCA was applied to all 18 maize root tissues included in the expanded atlas as described in Materials and Methods section. The percentage of variation among tissues explained by each principal component is displayed on both the *x*- (PC1) and *y* (PC2)-axes. Shape of points in the PCA plot denote major stages of development, with embryonic and postembryonic root tissues denoted with squares and triangles, respectively.

postembryonic root tissues sampled at the seventh and 13th vegetative stages (V7 and V13) as the coordinates of PC1 decrease. Strikingly, the root CP and stele—two adjoining tissues across the transversely sectioned root at the same developmental time point—are also divergently separated by PC2, indicating the extremely diverse functionality of these tissues. Overall, this analysis provides a glimpse into the distinct spatiotemporal biological functionality of the maize root.

Dynamic Reprogramming of the Maize Root Transcriptome

The maize root system has a unique, complex architecture that is responsible for the efficient uptake of water and nutrients, and also provides anchorage of the maize plant (Lynch, 1995; Aiken and Smucker, 1996). The root system of maize can be classified into two different groups: roots formed during embryogenesis and roots formed during postembryonic development (Hochholdinger and Tuberosa, 2009). The embryonic root system consists of a primary root formed at the basal pole of the embryo and a variable number of seminal roots at the scutellar node. The postembryonic root system is composed of shoot-born roots formed at consecutive shoot nodes and lateral roots stemming from the pericycle. Little is known about global transcriptional networks governing biological processes in embryonic and postembryonic root systems and temporal and spatial dynamics of such processes in maize. Clearly, such processes are under complex regulatory control, and elucidation of various components will be a crucial step toward improving root architecture. The tissues in the atlas were chosen to serve as a representative sample covering both the embryonic and postembryonic phases of maize root development (Fig. 1; Supplemental Fig. S4). A global look at the root transcriptome revealed that 70.6% (n = 27,873) of all annotated genes are expressed in at least one root tissue.

Since the morphology and functionality along the longitudinal axis of the maize primary root varies substantially (Ishikawa and Evans, 1995; Baluska et al., 1996; Hochholdinger et al., 2004), we profiled the dynamics of expression abundance along the proximal–distal gradient of the root. We divided the primary root into four zones: Zone 1, the meristematic zone, encompassing the first centimeter of the primary root, which harbors the root cap, root tip, quiescent center or stem cell niche, and the beginning of the elongation zone; Zone 2 includes the elongation zone and spans from the end of Zone 1 to the beginning of the differentiation zone; Zone 3 represents the lower, developmentally younger half of the differentiation zone characterized by the appearance of root hairs and lateral roots; and Zone 4 denotes the upper, developmentally older half of the differentiation zone (Fig. 1d).

Upon all possible pair-wise comparisons of the 27,873 genes expressed across the four longitudinal zones of the primary root, we identified 9347 (34%) of genes that were fourfold differentially expressed in one or more comparisons. Genes that exhibited fourfold expression variation for any pair-wise comparison across individual root zones were grouped by developmental dynamics using the K-means clustering algorithm. We

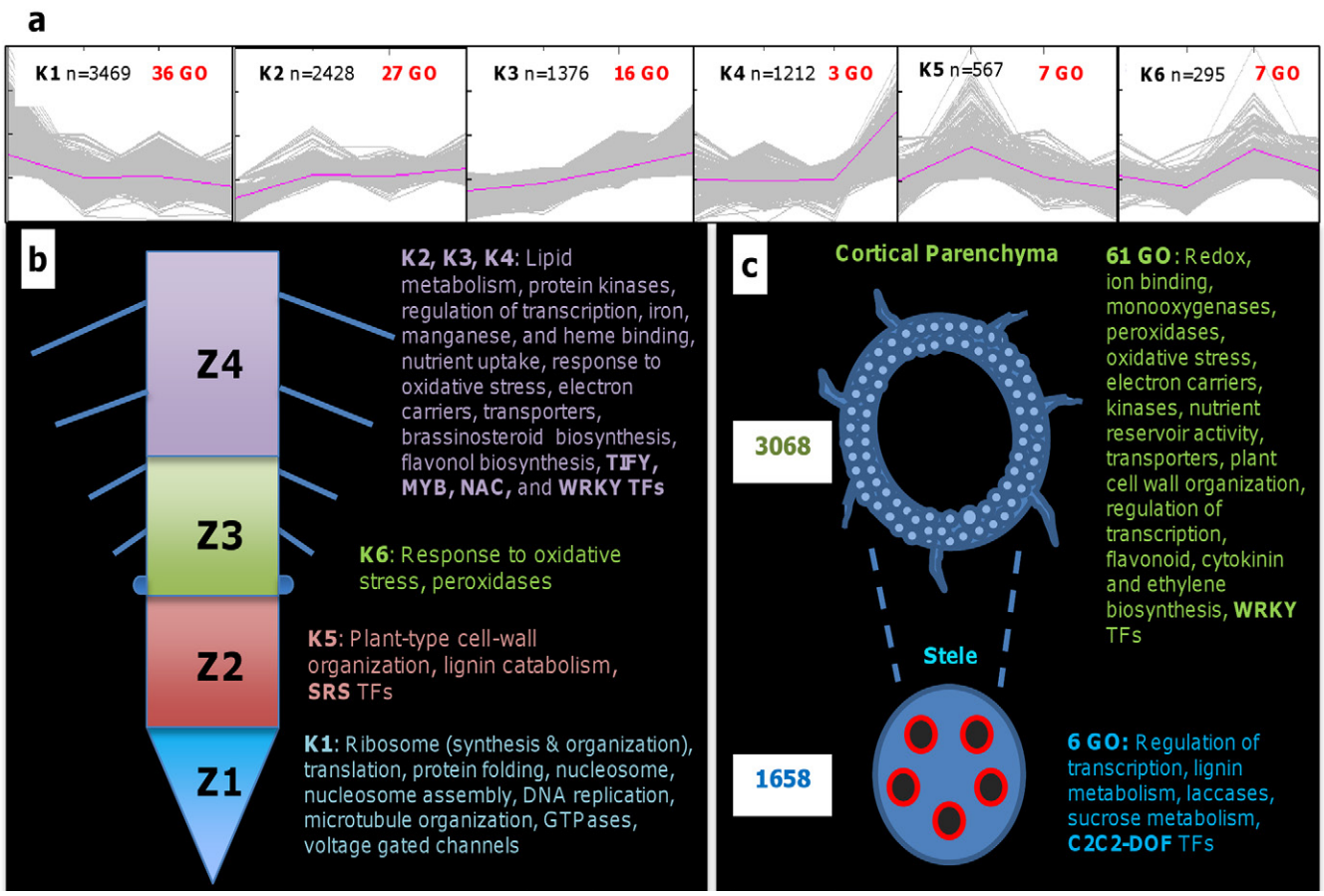

Figure 4. Spatiotemporal enrichment of biological processes within the maize root. (a) K-means coexpression clusters (K1–K6) of genes that vary by fourfold change across the longitudinal axis (Zones 1–4) of the maize primary root. Number of enriched gene ontology (GO) terms per cluster is shown in red and *n* denotes number of genes per cluster. Enriched GO terms of differentially expressed genes of (b) six K-means coexpression clusters, which vary across longitudinal zones (Zones 1–4) and (c) a pairwise comparison between radially separated cortical parenchyma (CP) and stele tissue. Numbers in the boxes represent the number of differentially expressed genes (fourfold) with highest gene expression corresponding to that zone. The lists of all significant GO term enrichments for the K-means clusters across longitudinal root zones and for the CP vs. stele comparison are included in Supplemental Table S4 and S5, respectively.

identified six clusters (K1–K6; Supplemental Dataset S5) with four main clusters (K1–K4) accounting for ~90% of the differentially expressed genes in the four root zones (Fig. 4a). We then used the gene lists from each K-means coexpression cluster for GO enrichment analysis, revealing that dynamic coexpression clusters represent distinct biological processes (Fig. 4b; Supplemental Table S4). For example, genes that encode enzymes for translation, ribosomal function and assembly, protein metabolism, DNA synthesis and replication, transcriptional activation, cell cycle regulation, microtubule motor activity, nucleosome assembly, and plant-type cell-wall organization are highly enriched in Cluster K1, which represents genes that are expressed at the highest levels in the root tip (Zone 1). These biological processes are consistent with functions of rapidly dividing cells in this broad meristematic zone. Interestingly, several of these same biological functions are also overrepresented in the leaf base (relative to the leaf tip), which, like the root tip, is an actively dividing, relatively undifferentiated tissue compared with the leaf tip (Li et al., 2010). Genes that show peak expression in the transitioning zones of the root (Zones 2 and 3) are represented by Clusters K5 and K6, which included those required for carbohydrate and lipid metabolic processes, response to oxidative stress, peroxidases, lignin catabolism, cell wall organization, and SRS transcription factors, a gene family shown to be involved with auxin-mediated lateral root primordia initiation in maize (Zhang et al., 2015). This is consistent with processes related to cell wall deposition and reorganization during root elongation and differentiation and initiation of structures such as root hairs and lateral roots to enhance nutrient uptake. Additionally, glutathione peroxidases, which are involved in reactive oxygen species (ROS)-related processes, have been shown to regulate root system architecture in *Arabidopsis* (Passaia et al., 2014). Finally, Clusters K2, K3, and K4 exhibit peak gene expression in Zone 4, representing the most differentiated zone of the root. This zone features predominant expression of genes that encode nutrient reservoir activity, transport, kinases, protein phosphorylation, regulation of transcription and TF activity (including enrichment for TIFY, MYB, NAC, and

WRKY families), monooxygenase activity, glutathione transferases, redox regulation, electron carrier activity, lipid metabolism, and biosynthesis of flavonoids. A significant enrichment of kinases and TFs at the initiation of the differentiation zone was also observed in *Arabidopsis* roots (Birnbaum et al., 2003), suggesting that extensive employment of signaling networks and transcriptional activity during cell maturation in these root zones is prevalent in plants. Redox regulation and ROS have been shown to be crucial for many forms of root functionality related to gravitropism, root hair initiation and elongation, lateral root development, stress response, and hormone regulation (Joo et al., 2001; Foreman et al., 2003; Carol and Dolan, 2006; Baxter et al., 2014; Manzano et al., 2014; Nestler et al., 2014). Together, these results reveal major biochemical shifts along the proximal–distal root gradient that are produced in part by highly dynamic, coordinated, and localized transitions in mRNA abundance.

Exploring the Cortical Parenchyma and Stele Transcriptomes

Intrigued by striking differences between the CP and stele transcriptome observed in the PCA, we focused on the dynamic expression of genes to elucidate the distinct biological processes between these two radially separated tissues. The CP is comprised of the endodermis, multiple layers of cortical tissue, and a single layer of epidermal tissue, and biologically, it is involved in the uptake and transport of nutrients (Saleem et al., 2010). Lying beneath the endodermal layer of the CP and surrounding the innermost pith parenchyma cells, the cylindrical-shaped stele encompasses the vascular system, which includes xylem for transporting water and nutrients and phloem for transporting photoassimilates (Hochholdinger and Tuberosa, 2009). While these tissues clearly play a key role in basic root function, transcriptional and biochemical underpinnings of their functionality are poorly understood (Saleem et al., 2010).

Of the 26,107 genes expressed in either the CP or stele, 88% were common, suggesting similar global transcriptomes. However, 4728 (18%) genes showed at least fourfold differential expression between the two tissues, which likely underlie the unique functionality between these tissues. The CP was transcriptionally and metabolically more active, with 3068 genes showing higher expression than 1658 genes up-regulated in the stele. This was also evident from GO enrichment analysis of differentially expressed genes between the CP and stele (Fig. 4c; Supplemental Table S5). The CP was enriched for 61 processes including heme binding, redox, monooxygenases, peroxidases, electron carriers, protein kinase activity, transporters, hydrolase activity, regulation of transcription and TF activity (particularly WRKY TFs), cell-wall organization, carbohydrate metabolic processes, nutrient reservoir activity, sexual reproduction, cytokinin-O-glucoside biosynthesis, flavonoid biosynthesis, and ethylene biosynthesis. Enrichment of several of these metabolic processes in the CP (particularly flavonoid biosynthesis and cell-wall modification) is also readily apparent from MapMan (Thimm et al., 2004; Usadel et al., 2009) analysis (Supplemental Fig. S5). Consistent with the enrichment of transporters and nutrient reservoir activity in the CP, the endodermis of the CP evolved as a key cell layer responsible for preventing the apoplastic passage of ions from the cortex to the stele as the suberized casparian strip facilitates selective transport of ions, nutrients, and water to the inner root cells. Enrichment of cytokinin-O-glucoside biosynthesis in the CP relative to the stele is consistent with preferential accumulation of cytokinin cis-zeatin, and its precursors and conjugates observed during hormone profiling of this tissue (Saleem et al., 2010). Cytokinins modulate root organogenesis by modulating polar auxin transport and inhibiting lateral root initiation in the differentiation zone (Esau, 1965; Laplaze et al., 2007). The enrichment of flavonoid biosynthesis genes in the CP is supported by metabolomic and gene expression analyses in *Arabidopsis* (Brady et al., 2007; Moussaieff et al., 2013); interestingly, flavonoids have been shown to exhibit antimicrobial properties imparting the plant to resist pathogens (Dixon et al., 2002; Dixon and Pasinetti, 2010). Prevalence of redox processes, monooxygenases, and peroxidases in the CP is consistent with their role in ROS signaling, which mediates the plants response to hypoxia and modulating aerenchyma and lateral root formation (Bouranis et al., 2006; Steffens et al., 2013). Enrichment of the GO term sexual reproduction is due to the overrepresentation of several extensin and expansin genes, consistent with the role of these enzymes in cell wall loosening required for root hair initiation and elongation from epidermal cells (Lin et al., 2011; ZhiMing et al., 2011). This term may also be enriched because of the common transcriptional network shared between root hair and pollen tube apical tip growth as has been shown in *Arabidopsis* (Becker et al., 2014). Similarly, the enrichment of ethylene biosynthesis is in agreement with its role in regulation of root elongation and enhancement of root hair growth (Tanimoto et al., 1995; Pitts et al., 1998; Le et al., 2001).

Enrichment of comparatively fewer biological processes in the stele (six GO terms) indicates this tissue is potentially more specialized relative to the CP. These processes included regulation of transcription, lignin catabolism, laccase activity, C2C2-Dof TF expression, and sucrose metabolism. Lignin catabolism and laccases activity are processes associated with vascular differentiation (Zhao et al., 2013; Schuetz et al., 2014). These terms are also overrepresented in the stele of the MapMan analysis of differentially expressed genes, depicted under the phenolics squares of secondary metabolism (Supplemental Fig. S5). Moreover, sucrose is a primary carbohydrate transported by phloem, and metabolism of sucrose into monosaccharides in the stele is essential for respiration (Izmailov et al., 1982).

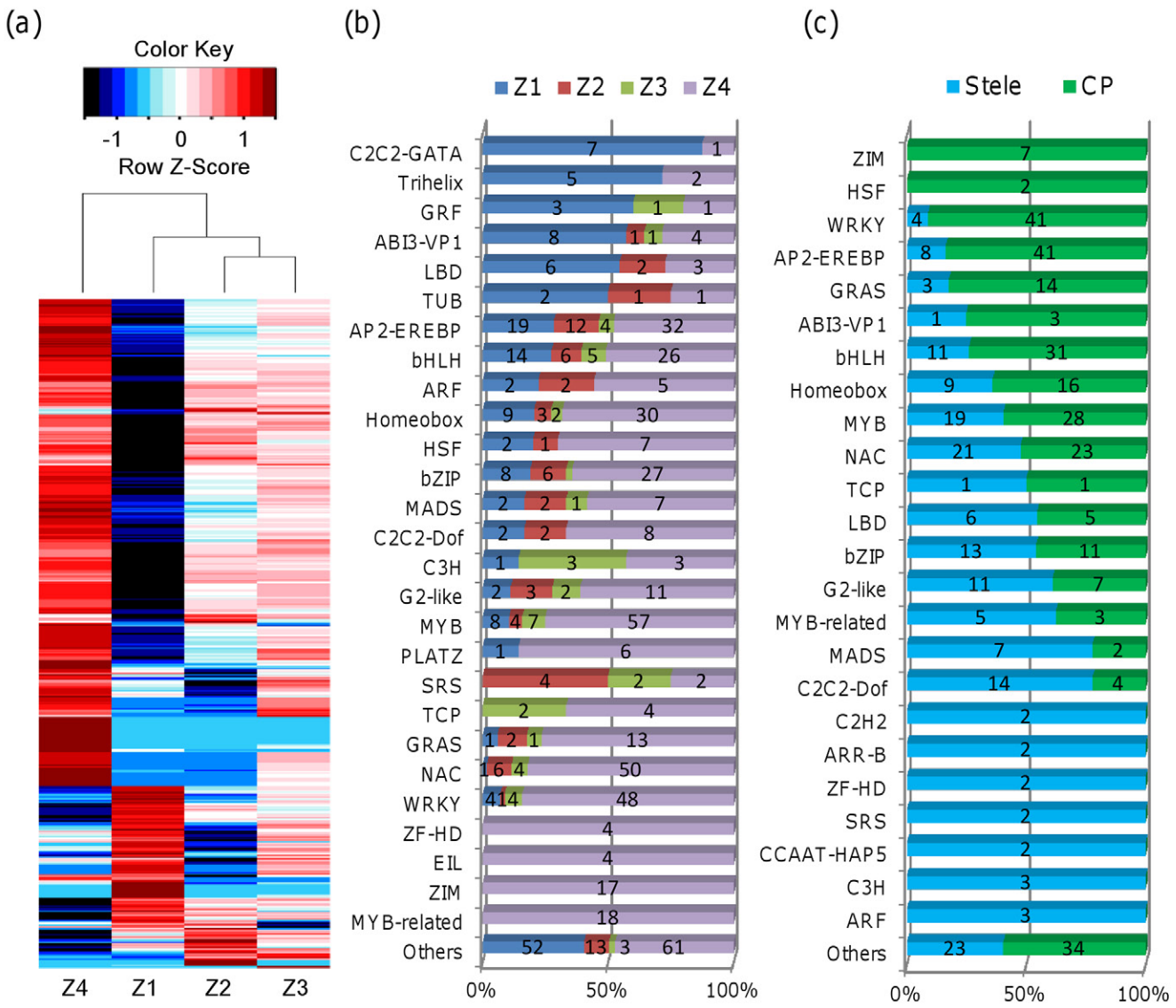

Figure 5. Dynamic inventories of transcription factors (TFs) orchestrate root development. (a) Heat map of hierarchical clustering of 762 differentially expressed (fourfold) TFs across all pair-wise comparisons of the longitudinal gradient of root. Heat map was clustered based on Euclidean distance, normalized with log2 transformation. The TFs were only included if they had an fragments per kb exon model per million mapped fragments (FPKM) > 1 in at least one tissue. (b) Distribution of differentially expressed TF families across all pair-wise comparisons of longitudinal zones of the primary root 7 d after sowing (DAS). (c) Distribution of differentially expressed TF families between the CP and stele, representing the transverse gradient of the primary root (3DAS). Numbers of genes exhibiting the highest values of gene expression for each TF family within a tissue are depicted.

Overall, GO enrichment analysis showed very disparate patterns of gene expression delineating the CP and stele tissues, which is consistent with distinct and coordinated biological functions performed by both tissues.

Comparing Biological Trends between the Root Transcriptome and Proteome

A recent study produced a high-resolution, maize-tissue-specific root proteome and phosphoproteome atlas along both the longitudinal and radial axes (Marcon et al., 2015). This study dissected maize primary roots of 2 to 4 cm in length, roughly equivalent to the physiological age of our Primary Root, CP, and stele 3DAS tissues, both longitudinally (meristematic zone, elongation zone, and differentiation zone) and radially (divided differentiation zone into cortical parenchyma and stele). Gene ontology enrichment analysis of tissue-specific proteins identified two gradients reflecting abundance of functional protein classes along the longitudinal axis: GO terms related to RNA, DNA, and protein peaked in the meristematic zone, while the classes related to cell wall, lipid metabolism, stress, transport, and secondary metabolism accumulated in the differentiation zone (Marcon et al., 2015). Similar to proteomic gradients along the longitudinal axis, the same pattern could be found in our longitudinal root (Z1–Z4) K-means coexpression clusters, even though we used a slightly more mature root system (Fig. 4a, 5b). Additionally, Marcon et al. conducted GO

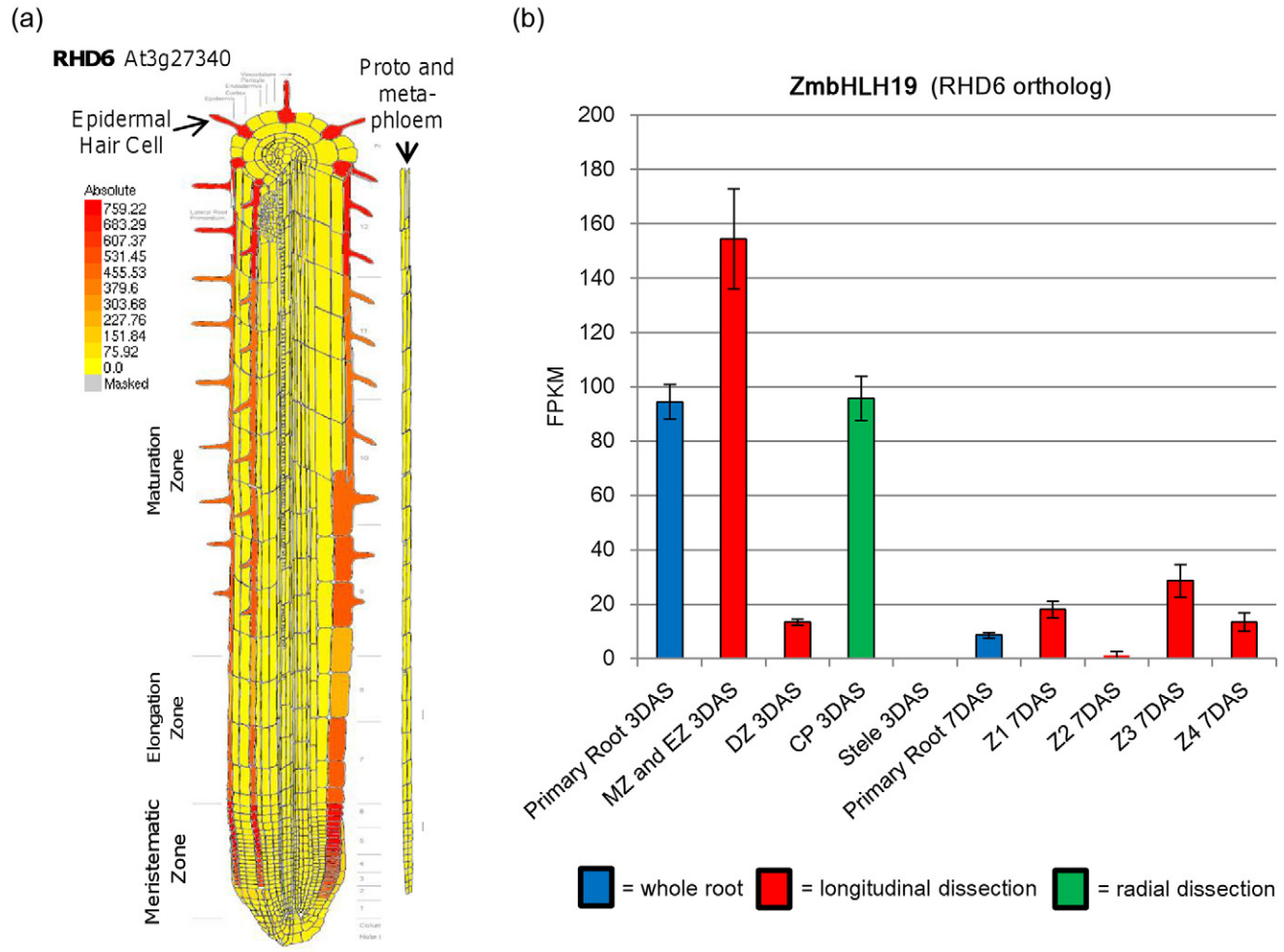

Figure 6. Enhanced tissue-specific resolution provided by the gene atlas facilitates evaluation of candidate gene functionality using a cross-species genomics approach. Similar spatiotemporal gene expression patterns are shared between the *Arabidopsis* gene ROOT HAIR DEFECTIVE 6 (RHD6) (a), which modulates root hair initiation and elongation, and its maize ortholog, ZmbHLH19, pictured in (b). *Arabidopsis* root spatiotemporal cell-type specific microarray expression data shown in (a) was published previously (Brady et al., 2007) and visualized pictorially with the Arabidopsis eFP browser (Winter et al., 2007).

single-enrichment analysis on CP (n = 384) and stele (n = 305) specific, nonphosphorylated proteins via AgriGO (Du et al., 2010) and identified nine and 18 significantly enriched GO terms, respectively. Using the same enrichment tool on fourfold upregulated genes in the CP vs. stele from our transcriptome dataset, we identified 9 out of 9 and 14 out of 18 of the identical, significantly enriched GO terms from the CP and stele proteomic analysis (85.2% agreement in total), indicating that major biological trends between protein and transcript accumulation are concordant (Supplemental Table S6). Although we could not accurately compare our quantitative RNA-seq data to the proteomics data of Marcon et al. in light of differences in growth methods, sequencing technologies, read depth, bioinformatics methods, etc., Marcon et al. previously compared protein levels with RNA-seq data from their own laboratory on the same tissues (Paschold et al., 2014) and found moderately positive Pearson's correlations between mRNA and protein (r = 0.38 for both CP and stele tissues). A previous study examining mRNA–protein correlations in maize endosperm and embryo reported a similar relationship (r = 0.41), which they attributed to posttranscriptional regulation of protein abundance, translational inhibition or targeted protein degradation (Walley et al., 2013). Together, these observations highlight the importance of a comprehensive systems approach involving all components of the central dogma (genome, transcriptome, proteome, metabolome, and phenome) to better understand the biology of an organism.

Changing Inventories of Transcription Factors Orchestrate Root Development

The dynamics of TF expression during cellular differentiation along the root axis were particularly well resolved in our RNA-seq data. Of the 2630 TFs belonging to 47 families described at GRASSIUS (http://grassius.org) and elsewhere (Yilmaz et al., 2009), 1736 (74%) were detected in primary root tissue, with 762 (29%) exhibiting fourfold differential expression along the longitudinal developmental gradient (Fig. 6a). Most of these genes (68%) were expressed at the highest levels in the most

developed and differentiated portion of the root (Zone 4), whereas only 20% were expressed at the highest levels in the root tip (Zone 1). An additional 9% of TFs showed peak expression in the elongation zone (Zone 2) and 6% peaked in Zone 3, the younger half of the differentiation zone. Interestingly, this pattern of peak expression of TFs in the most differentiated and functional root zone is the opposite pattern relative to a gradient of leaf development from base to tip, where TF expression peaked in the undifferentiated base of the leaf relative to the less differentiated leaf tip (Li et al., 2010). Hierarchical clustering analysis indicated that TF accumulation was most similar between the transition zones of Z2 and Z3, and, as expected, most divergent between Z1 and Z4 (Fig. 5a). Further examination of TF families showed that specific families were predominant in different longitudinal root zones (Fig. 5b). The TIFY, NAC, MYB, and WRKY families of transcriptional regulators were highly expressed in the upper differentiation zone (Zone 4), likely orchestrating diverse functions related to stress responses, plant defense, nutrient uptake, and lateral root and root hair formation. Additionally, the TIFY, MYB-related, and EIL families were restricted to the upper differentiation zone. The TIFY family (previously known as ZIM) regulates root elongation by controlling jasmonate signaling (Cheng et al., 2011), while the EIL family is involved in ethylene signaling, which enhances lateral root and root hair formation (Pitts et al., 1998; Potuschak et al., 2003; Binder et al., 2007)

We also detected TFs that were differentially expressed between the CP and stele and identified 232 enriched in CP and 146 in stele. The TIFY, WRKY, and AP2-EREBP, and GRAS TFs were enriched in the CP while ARF, C2C2-Dof, MADS, and G2-like TFs were enriched in stele (Fig. 5c). The enrichment of GRAS TFs in the CP is interesting, as the master GRAS TF, *SCARECROW*, which exhibits localized gene expression in the endodermis and cortex of the CP, regulates an asymmetric cell division essential for generating the radial organization of the *Arabidopsis* root (Di Laurenzio et al., 1996; Wysocka-Diller et al., 2000). The C2C2-Dof and G2-like TFs have also been shown to be overrepresented in phloem cells in *Arabidopsis* (Mustroph et al., 2009), suggesting a similar role related to the functionality of this conductive vascular tissue.

The ability to examine gene expression in both longitudinal and radial gradients of the root permitted us to more effectively probe several tissue-specific TFs, which are supported by previously published evidence, thus implicating them as interesting candidates warranting further exploration. To highlight the utility of the dataset, we compared expression profiles of a few interesting TFs previously identified and characterized in the *Arabidopsis* root (Brady et al., 2007) and visualized expression of these TFs with the *Arabidopsis* eFP browser (Winter et al., 2007). We compared spatiotemporal gene expression of these *Arabidopsis* TFs with gene expression of their corresponding maize orthologs within our dataset and observed similar spatiotemporal gene expression patterns. For instance, maize gene *ZmbHLH19* (GRMZM2G066057) is an ortholog of the *Arabidopsis* gene ROOT HAIR DEFECTIVE 6 (*RHD6*), which modulates root hair initiation and elongation through auxin and ethylene mediated processes. In *Arabidopsis*, *RHD6* accumulates in trichoblasts (future hair cells) of the meristem, in the elongation zone just before hair outgrowth, and during hair growth itself and ceases expression concurrent with hair growth (Yi et al., 2010) (Fig. 6a). Interestingly, in maize, *ZmbHLH19* exhibited a similar expression radially localized to the CP, which harbors the epidermis and longitudinally peaks in Zone 3 of the primary root (Fig. 6b), thus implicating gene expression to a region of root hair initiation and elongation.

Likewise, a stele-specific TF (relative to the CP) encoding maize gene *ZmGLK53* (GRMZM2G052544) and its *Arabidopsis* ortholog *ALTERED PHLOEM DEVELOPMENT* (*APL*), which governs phloem poles and sieve element differentiation while simultaneously inhibiting xylem development (Bonke et al., 2003), showed similar expression patterns. Expression of *APL* is limited to protophloem, metaphloem, and to a lesser extent in phloem companion cells, and increases with aging of the longitudinal gradient of the root (Brady et al., 2007). *ZmGLK53* exhibits a similar expression pattern, being completely localized to the stele radially with its expression steadily increasing along the longitudinal axis from Zone 1 through Zone 4 (Supplemental Fig. S6a,b).

Finally, *Arabidopsis LBD16*, which regulates lateral root development, is specifically expressed in the root stele and lateral root primordia, which initiate from the pericycle cell layer contained within the stele (Okushima et al., 2007). The maize ortholog of LBD16, encoded by *ZmLBD24* (GRMZM2G075499), also exhibits both radial and longitudinal expression biases within the maize root. Radially, *ZmLBD24* is also highly expressed in the stele relative to the CP (17-fold higher), and longitudinally across four root zones this TF exhibits drastically higher expression in Zone 2, which harbors the elongation zone and ends immediately before the point of lateral root initiation (Supplemental Fig. S6c,d), thus likely regulating lateral root initiation in maize. Taken together, the enhanced resolution of tissues in the RNA-seq dataset provided in our current study will facilitate evaluation of gene functionality using a cross-species genomics approach to evaluate candidate genes in maize.

Availability of the Maize Transcriptome

To facilitate gene discovery and functional genomics of maize and related grasses, this comprehensive RNA-seq-based transcriptome is available to the community at Maize Genetics and Genomics Database (MaizeGDB; www.maizeGDB.org) (Lawrence et al., 2004) for easy visualization. Matrices of FPKM values at both the individual gene model (Supplemental Dataset S1, S2) and transcript

level (Supplemental Dataset S3, S4), along with physical location, are provided as supplemental datasets. The raw sequence reads have been deposited in the National Center for Biotechnology Information Sequence Read Archive (accession numbers PRJNA171684 and SRP010680).

CONCLUSIONS

In this study, we have performed transcriptional analysis of 79 representative maize tissues, capturing important aspects of maize development using RNA-seq. We have demonstrated that the dataset is of high quality and that the results of biological replicates are highly reproducible. This dataset provides enhanced spatiotemporal coverage of the transcriptome as a result of the substantial number of tissues included, creating the most extensive coordinated maize transcriptome dataset to date. We highlighted the utility of this new RNA-seq dataset to understand the biological specification of two radially separated and diverse root tissues, the CP and stele, and to provide insights into seedling root development. In conclusion, this comprehensive RNA-seq dataset that we have generated is expected to be a powerful tool in understanding maize development, physiology, and phenotypic diversity.

Supporting Information

Figure S1. Images corresponding to all tissues included from the original microarray-based gene atlas and a previous senescence study.

Figure S2. Nomenclature of postembryonic root nodes sampled.

Figure S3. Total number of expressed genes across all tissues.

Figure S4. Principal component analysis (PCA) of all 79 tissues represented in the expanded RNA-seq gene expression atlas.

Figure S5. MapMan view of overall cell metabolism differences in gene expression between the CP and stele.

Figure S6. Examples of enhanced tissue-specific resolution provided by the gene atlas facilitating candidate gene evaluation using a cross-species genomics approach.

Table S1. Sequencing information for all tissue sample replicates included in the study.

Table S2. Pairwise correlations between bioreplications of tissue samples.

Table S3. Gene Ontology (GO) enrichment analysis of non-expressed genes in the RNA-seq gene atlas.

Table S4. Enriched biological terms of six k-means co-expression clusters across longitudinal root zones (Z1-Z4).

Table S5. Significantly enriched Gene Ontology (GO) terms from PlantGSEA for fourfold differentially expressed genes between the CP and stele.

Table S6. Comparison of enriched Gene Ontology (GO) terms between CP and stele transcriptome and proteome data.

Dataset S1. Matrix of mean expression values (FPKMs) on a per gene basis for all tissues published in the study.

Dataset S2. Matrix of expression values (FPKMs) for each bioreplication on a per gene basis for all tissues published in the study.

Dataset S3. Matrix of mean expression values (FPKMs) on a transcript basis for all tissues published in the study.

Dataset S4. Matrix of expression values (FPKMs) for each bioreplication on a transcript basis for all tissues published in the study.

Dataset S5. List of K-means co-expression clusters across longitudinal root zones.

Acknowledgments

This work was funded by the Department of Energy Great Lakes Bioenergy Research Center (Department of Energy Office of Biological and Environmental Research grant number DE-FC02-07ER64494), the National Science Foundation's (NSF) Basic Research to Enable Agricultural Development (BREAD) program (0965480), and Agriculture and Food Research Initiative of the U.S. Department of Agriculture National Institute of Food and Agriculture (grant no. 2014-67013-2157). The authors thank the MaizeGDB team of Jack Gardiner, Mary Schaeffer, Carson Andorf, and John Portwood for making this resource easily visualized and utilized by the plant community. S.C.S was supported in part by the National Institute of Food and Agriculture, USDA Hatch funding (WIS01645). The authors declare no conflict of interest.

References

Aiken, R.M., and A.J.M. Smucker. 1996. Root system regulation of whole plant growth. Annu. Rev. Phytopathol. 34:325–346. doi:10.1146/annurev.phyto.34.1.325

Baluska, F., D. Volkmann, and P.W. Barlow. 1996. Specialized zones of development in roots: View from the cellular level. Plant Physiol. 112:3.

Baxter, A., R. Mittler, and N. Suzuki. 2014. ROS as key players in plant stress signalling. J. Exp. Bot. 65:1229–1240. doi:10.1093/jxb/ert375

Becker, J.D., S. Takeda, F. Borges, L. Dolan, and J.A. Feijó. 2014. Transcriptional profiling of Arabidopsis root hairs and pollen defines an apical cell growth signature. BMC Plant Biol. 14:197. doi:10.1186/s12870-014-0197-3

Benedito, V.A., I. Torres-Jerez, J.D. Murray, A. Andriankaja, S. Allen, K. Kakar, et al. 2008. A gene expression atlas of the model legume *Medicago truncatula*. Plant J. 55:504–513. doi:10.1111/j.1365-313X.2008.03519.x

Benjamini, Y., and D. Yekutieli. 2001. The control of the false discovery rate in multiple testing under dependency. Ann. Stat. 29:1165–1188.

Binder, B.M., J.M. Walker, J.M. Gagne, T.J. Emborg, G. Hemmann, A.B. Bleecker, et al. 2007. The Arabidopsis EIN3 binding F-Box proteins EBF1 and EBF2 have distinct but overlapping roles in ethylene signaling. The Plant Cell Online 19:509–523. doi:10.1105/tpc.106.048140

Birnbaum, K., D.E. Shasha, J.Y. Wang, J.W. Jung, G.M. Lambert, D.W. Galbraith, et al. 2003. A gene expression map of the Arabidopsis root. Science 302:1956–1960. doi:10.1126/science.1090022

Bonke, M., S. Thitamadee, A.P. Mähönen, M.-T. Hauser, and Y. Helariutta. 2003. APL regulates vascular tissue identity in Arabidopsis. Nature 426:181–186. doi:10.1038/nature02100

Bouranis, D.L., S.N. Chorianopoulou, C. Kollias, P. Maniou, V.E. Protonotarios, V.F. Siyiannis, et al. 2006. Dynamics of aerenchyma distribution in the cortex of sulfate-deprived adventitious roots of maize. Ann. Bot. (Lond.) 97:695–704. doi:10.1093/aob/mcl024

Brady, S.M., D.A. Orlando, J.Y. Lee, J.Y. Wang, J. Koch, J.R. Dinneny, et al. 2007. A high-resolution root spatiotemporal map reveals dominant expression patterns. Science 318:801–806. doi:10.1126/science.1146265

Brown, P.J., N. Upadyayula, G.S. Mahone, F. Tian, P.J. Bradbury, S. Myles, et al. 2011. Distinct genetic architectures for male and female inflorescence traits of maize. PLoS Genet. 7:E1002383. doi:10.1371/journal.pgen.1002383

Carol, R.J., and L. Dolan. 2006. The role of reactive oxygen species in cell growth: Lessons from root hairs. J. Exp. Bot. 57:1829–1834. doi:10.1093/jxb/erj201

Chen, J., B. Zeng, M. Zhang, S. Xie, G. Wang, A. Hauck, et al. 2014. Dynamic transcriptome landscape of maize embryo and endosperm development. Plant Physiol. 166:252–264. doi:10.1104/pp.114.240689

Cheng, Z., L. Sun, T. Qi, B. Zhang, W. Peng, Y. Liu, et al. 2011. The bHLH transcription factor MYC3 interacts with the jasmonate ZIM-domain proteins to mediate jasmonate response in *Arabidopsis*. Mol. Plant 4:279–288. doi:10.1093/mp/ssq073

Davidson, R.M., C.N. Hansey, M. Gowda, K.L. Childs, H. Lin, B. Vaillancourt, et al. 2011. Utility of RNA sequencing for analysis of maize reproductive transcriptomes. Plant Gen. 4:191–203. doi:10.3835/plantgenome2011.05.0015

Di Laurenzio, L., J. Wysocka-Diller, J.E. Malamy, L. Pysh, Y. Helariutta, G. Freshour, et al. 1996. The SCARECROW gene regulates an asymmetric cell division that is essential for generating the radial organization of the Arabidopsis root. Cell 86:423–433. doi:10.1016/S0092-8674(00)80115-4

Dixon, R.A., L. Achnine, P. Kota, C.J. Liu, M. Reddy, and L. Wang. 2002. The phenylpropanoid pathway and plant defence—A genomics perspective. Mol. Plant Pathol. 3:371–390. doi:10.1046/j.1364-3703.2002.00131.x

Dixon, R.A., and G.M. Pasinetti. 2010. Flavonoids and isoflavonoids: From plant biology to agriculture and neuroscience. Plant Physiol. 154:453–457. doi:10.1104/pp.110.161430

Druka, A., G. Muehlbauer, I. Druka, R. Caldo, U. Baumann, N. Rostoks, et al. 2006. An atlas of gene expression from seed to seed through barley development. Funct. Integr. Genomics 6:202–211. doi:10.1007/s10142-006-0025-4

Du, Z., X. Zhou, Y. Ling, Z. Zhang, and Z. Su. 2010. agriGO: A GO analysis toolkit for the agricultural community. Nucleic Acids Res. 38:W64–W70. doi:10.1093/nar/gkq310

Esau, K. 1965. Plant anatomy 2nd ed. McGraw-Hill, New York.

Eveland, A.L., A. Goldshmidt, M. Pautler, K. Morohashi, C. Liseron-Monfils, M.W. Lewis, et al. 2014. Regulatory modules controlling maize inflorescence architecture. Genome Res. 24:431–443. doi:10.1101/gr.166397.113

Foreman, J., V. Demidchik, J.H. Bothwell, P. Mylona, H. Miedema, M.A. Torres, et al. 2003. Reactive oxygen species produced by NADPH oxidase regulate plant cell growth. Nature 422:442–446. doi:10.1038/nature01485

Grabherr, M.G., B.J. Haas, M. Yassour, J.Z. Levin, D.A. Thompson, I. Amit, et al. 2011. Full-length transcriptome assembly from RNA-Seq data without a reference genome. Nat. Biotechnol. 29:644–652. doi:10.1038/nbt.1883

Hochholdinger, F., and R. Tuberosa. 2009. Genetic and genomic dissection of maize root development and architecture. Curr. Opin. Plant Biol. 12:172–177. doi:10.1016/j.pbi.2008.12.002

Hochholdinger, F., K. Woll, M. Sauer, and D. Dembinsky. 2004. Genetic dissection of root formation in maize (*Zea mays*) reveals root-type specific developmental programmes. Ann. Bot. (Lond.) 93:359–368. doi:10.1093/aob/mch056

Ishikawa, H., and M.L. Evans. 1995. Specialized zones of development in roots. Plant Physiol. 109:725–727.

Izmailov, S., V. Piskorskaya, R. Bruskova, and A. Smirnov. 1982. Tissue specificity of assimilation and transport of nitrogen in the root of *Zea mays* L. seedlings. I. Transformations of 14C-sucrose and the nitrogen metabolism enzymes in cortex and stele. Biol. Plant. 24:241–247. doi:10.1007/BF02879452

Jiao, Y., S.L. Tausta, N. Gandotra, N. Sun, T. Liu, N.K. Clay, et al. 2009. A transcriptome atlas of rice cell types uncovers cellular, functional and developmental hierarchies. Nat. Genet. 41:258–263. doi:10.1038/ng.282

Joo, J.H., Y.S. Bae, and J.S. Lee. 2001. Role of auxin-induced reactive oxygen species in root gravitropism. Plant Physiol. 126:1055–1060. doi:10.1104/pp.126.3.1055

Komili, S., and P.A. Silver. 2008. Coupling and coordination in gene expression processes: A systems biology view. Nat. Rev. Genet. 9:38–48. doi:10.1038/nrg2223

Laplaze, L., E. Benkova, I. Casimiro, L. Maes, S. Vanneste, R. Swarup, et al. 2007. Cytokinins act directly on lateral root founder cells to inhibit root initiation. Plant Cell 19:3889–3900. doi:10.1105/tpc.107.055863

Lawrence, C.J., Q. Dong, M.L. Polacco, T.E. Seigfried, and V. Brendel. 2004. MaizeGDB, the community database for maize genetics and genomics. Nucleic Acids Res. 32:D393–D397. doi:10.1093/nar/gkh011

Le, J., F. Vandenbussche, D. Van Der Straeten, and J.P. Verbelen. 2001. In: the early response of Arabidopsis roots to ethylene, cell elongation is up-and down-regulated and uncoupled from differentiation. Plant Physiol. 125:519–522. doi:10.1104/pp.125.2.519

Li, G., D. Wang, R. Yang, K. Logan, H. Chen, S. Zhang, et al. 2014. Temporal patterns of gene expression in developing maize endosperm identified through transcriptome sequencing. Proc. Natl. Acad. Sci. USA 111:7582–7587. doi:10.1073/pnas.1406383111

Li, P., L. Ponnala, N. Gandotra, L. Wang, Y. Si, S.L. Tausta, et al. 2010. The developmental dynamics of the maize leaf transcriptome. Nat. Genet. 42:1060–1067. doi:10.1038/ng.703

Libault, M., A. Farmer, T. Joshi, K. Takahashi, R.J. Langley, L.D. Franklin, et al. 2010. An integrated transcriptome atlas of the crop model *Glycine max*, and its use in comparative analyses in plants. Plant J. 63:86–99. doi:10.1111/j.1365-313X.2010.04222.x

Lin, C., H.S. Choi, and H.T. Cho. 2011. Root hair-specific EXPANSIN A7 is required for root hair elongation in Arabidopsis. Mol. Cells 31:393–397. doi:10.1007/s10059-011-0046-2

Lynch, J. 1995. Root architecture and plant productivity. Plant Physiol. 109:7–13. doi:10.1104/pp.109.1.7

Manzano, C., M. Pallero, I. Casimiro, B. De Rybel, B. Orman-Ligeza, G. Van Isterdael, et al. 2014. The emerging role of ROS signalling during lateral root development. Plant Physiol. 3:1105–1119. doi:10.1104/pp.114.238873

Marcon, C., W.A. Malik, J.W. Walley, Z. Shen, A. Paschold, L.G. Smith, et al. 2015. A high resolution tissue-specific proteome and phosphoproteome atlas of maize primary roots reveals functional gradients along the root axis. Plant Physiol. 168:233–46 doi:10.1104/pp.15.00138

Martin, J.A., N.V. Johnson, S.M. Gross, J. Schnable, X. Meng, M. Wang et al. 2014. A near complete snapshot of the *Zea mays* seedling transcriptome revealed from ultra-deep sequencing. Scientific Reports 4:4519.

Mortazavi, A., B.A. Williams, K. McCue, L. Schaeffer, and B. Wold. 2008. Mapping and quantifying mammalian transcriptomes by RNA-Seq. Nat. Methods 5:621–628. doi:10.1038/nmeth.1226

Moussaieff, A., I. Rogachev, L. Brodsky, S. Malitsky, T.W. Toal, H. Belcher, et al. 2013. High-resolution metabolic mapping of cell types in plant roots. Proc. Natl. Acad. Sci. USA 110:E1232–E1241. doi:10.1073/pnas.1302019110

Mustroph, A., M.E. Zanetti, C.J. Jang, H.E. Holtan, P.P. Repetti, D.W. Galbraith, et al. 2009. Profiling translatomes of discrete cell populations resolves altered cellular priorities during hypoxia in Arabidopsis. Proc. Natl. Acad. Sci. USA 106:18843–18848. doi:10.1073/pnas.0906131106

Nestler, J., S. Liu, T.J. Wen, A. Paschold, C. Marcon, H.M. Tang, et al. 2014. Roothairless5, which functions in maize (*Zea mays* L.) root hair initiation and elongation encodes a monocot-specific NADPH oxidase. Plant J. 79:729–740. doi:10.1111/tpj.12578

Okoniewski, M.J., and C.J. Miller. 2006. Hybridization interactions between probesets in short oligo microarrays lead to spurious correlations. BMC Bioinformatics 7:276. doi:10.1186/1471-2105-7-276

Okushima, Y., H. Fukaki, M. Onoda, A. Theologis, and M. Tasaka. 2007. ARF7 and ARF19 regulate lateral root formation via direct activation of LBD/ASL genes in Arabidopsis. The Plant Cell Online 19:118–130. doi:10.1105/tpc.106.047761

Paschold, A., N.B. Larson, C. Marcon, J.C. Schnable, C.T. Yeh, C. Lanz, et al. 2014. Nonsyntenic genes drive highly dynamic complementation of gene expression in maize hybrids. Plant Cell 26:3939–3948. doi:10.1105/tpc.114.130948

Passaia, G., G. Queval, J. Bai, M. Margis-Pinheiro, and C.H. Foyer. 2014. The effects of redox controls mediated by glutathione peroxidases on root architecture in Arabidopsis thaliana. J. Exp. Bot. 65:1403–1413. doi:10.1093/jxb/ert486

Pitts, R.J., A. Cernac, and M. Estelle. 1998. Auxin and ethylene promote root hair elongation in Arabidopsis. Plant J. 16:553–560. doi:10.1046/j.1365-313x.1998.00321.x

Potuschak, T., E. Lechner, Y. Parmentier, S. Yanagisawa, S. Grava, C. Koncz, et al. 2003. EIN3-dependent regulation of plant ethylene hormone signaling by two Arabidopsis F box proteins: EBF1 and EBF2. Cell 115:679–689. doi:10.1016/S0092-8674(03)00968-1

R Core Development Team. 2014. R: A language and environment for statistical computing. R Foundation for Statistical Computing, Vienna, Austria.

Royce, T.E., J.S. Rozowsky, and M.B. Gerstein. 2007. Toward a universal microarray: Prediction of gene expression through nearest-neighbor probe sequence identification. Nucleic Acids Res. 35:E99. doi:10.1093/nar/gkm549

Saleem, M., T. Lamkemeyer, A. Schützenmeister, J. Madlung, H. Sakai, H.P. Piepho et al. 2010. Specification of cortical parenchyma and stele of maize primary roots by asymmetric levels of auxin, cytokinin, and cytokinin-regulated proteins. Plant Physiology 152: 4–18. doi:10.1104/pp.109.150425

Schmid, M., T.S. Davison, S.R. Henz, U.J. Pape, M. Demar, M. Vingron, et al. 2005. A gene expression map of *Arabidopsis thaliana* development. Nat. Genet. 37:501–506. doi:10.1038/ng1543

Schnable, P.S., D. Ware, R.S. Fulton, J.C. Stein, F. Wei, S. Pasternak, et al. 2009. The B73 maize genome: Complexity, diversity, and dynamics. Science 326:1112–1115. doi:10.1126/science.1178534

Schuetz, M., A. Benske, R.A. Smith, Y. Watanabe, Y. Tobimatsu, J. Ralph, et al. 2014. Laccases direct lignification in the discrete secondary cell wall domains of protoxylem. Plant Physiol. 166:798–807. doi:10.1104/pp.114.245597

Sekhon, R.S., R. Briskine, C.N. Hirsch, C.L. Myers, N.M. Springer, C.R. Buell, et al. 2013. Maize gene atlas developed by RNA sequencing and comparative evaluation of transcriptomes based on RNA sequencing and microarrays. PLoS ONE 8:E61005. doi:10.1371/journal.pone.0061005

Sekhon, R.S., K. Childs, N. Santoro, C. Foster, C.R. Buell, N. de Leon, et al. 2012. Transcriptional and metabolic analysis of senescence induced by preventing pollination in maize. Plant Physiol. 159:1730–1744. doi:10.1104/pp.112.199224

Sekhon, R.S., H. Lin, K.L. Childs, C.N. Hansey, C.R. Buell, N. de Leon, et al. 2011. Genome-wide atlas of transcription during maize development. Plant J. 66:553–563. doi:10.1111/j.1365-313X.2011.04527.x

Shakoor, N., R. Nair, O. Crasta, G. Morris, A. Feltus, and S. Kresovich. 2014. A Sorghum bicolor expression atlas reveals dynamic genotype-specific expression profiles for vegetative tissues of grain, sweet and bioenergy sorghums. BMC Plant Biol. 14:35. doi:10.1186/1471-2229-14-35

Steffens, B., A. Steffen-Heins, and M. Sauter. 2013. Reactive oxygen species mediate growth and death in submerged plants. Front. Plant Sci. 4:179.

Sultan, M., M.H. Schulz, H. Richard, A. Magen, A. Klingenhoff, M. Scherf, et al. 2008. A global view of gene activity and alternative splicing by deep sequencing of the human transcriptome. Science 321:956–960. doi:10.1126/science.1160342

Tanimoto, M., K. Roberts, and L. Dolan. 1995. Ethylene is a positive regulator of root hair development in *Arabidopsis thaliana*. Plant J. 8:943–948. doi:10.1046/j.1365-313X.1995.8060943.x

Thimm, O., O. Bläsing, Y. Gibon, A. Nagel, S. Meyer, P. Krüger, et al. 2004. MAPMAN: A user-driven tool to display genomics data sets onto diagrams of metabolic pathways and other biological processes. Plant J. 37:914–939. doi:10.1111/j.1365-313X.2004.02016.x

Thompson, B.E., and S. Hake. 2009. Translational biology: From Arabidopsis flowers to grass inflorescence architecture. Plant Physiol. 149:38–45. doi:10.1104/pp.108.129619

Tomcal, M., N. Stiffler, and A. Barkan. 2013. POGs2: A web portal to facilitate cross-species inferences about protein architecture and function in plants. PLoS ONE 8:E82569. doi:10.1371/journal.pone.0082569

Usadel, B., F. Poree, A. Nagel, M. Lohse, A. Czedik-Eysenberg, and M. Stitt. 2009. A guide to using MapMan to visualize and compare Omics data in plants: A case study in the crop species, Maize. Plant Cell Environ. 32:1211–1229. doi:10.1111/j.1365-3040.2009.01978.x

Verdier, J., I. Torres-Jerez, M. Wang, A. Andriankaja, S.N. Allen, J. He, et al. 2013. Establishment of the *Lotus japonicus* Gene Expression Atlas (LjGEA) and its use to explore legume seed maturation. Plant J. 74:351–362. doi:10.1111/tpj.12119

Vollbrecht, E., and R.J. Schmidt. 2009. Development of the inflorescences. Handbook of maize: Its biology. Springer, New York. p. 13–40.

Walker, N.S., N. Stiffler, and A. Barkan. 2007. POGs/PlantRBP: A resource for comparative genomics in plants. Nucleic Acids Res. 35:D852–D856. doi:10.1093/nar/gkl795

Walley, J.W., Z. Shen, R. Sartor, K.J. Wu, J. Osborn, L.G. Smith, et al. 2013. Reconstruction of protein networks from an atlas of maize seed proteotypes. Proc. Natl. Acad. Sci. USA 110:E4808–E4817. doi:10.1073/pnas.1319113110

Wang, Z., M. Gerstein, and M. Snyder. 2009. RNA-Seq: A revolutionary tool for transcriptomics. Nat. Rev. Genet. 10:57–63. doi:10.1038/nrg2484

Winter, D., B. Vinegar, H. Nahal, R. Ammar, G.V. Wilson, and N.J. Provart. 2007. An "Electronic Fluorescent Pictograph" browser for exploring and analyzing large-scale biological data sets. PLoS ONE 2:E718. doi:10.1371/journal.pone.0000718

Wysocka-Diller, J.W., Y. Helariutta, H. Fukaki, J.E. Malamy, and P.N. Benfey. 2000. Molecular analysis of SCARECROW function reveals a radial patterning mechanism common to root and shoot. Development 127:595–603.

Yi, K., B. Menand, E. Bell, and L. Dolan. 2010. A basic helix-loop-helix transcription factor controls cell growth and size in root hairs. Nat. Genet. 42:264–267. doi:10.1038/ng.529

Yi, X., Z. Du, and Z. Su. 2013. PlantGSEA: A gene set enrichment analysis toolkit for plant community. Nucleic Acids Res. 41:W98–W103. doi:10.1093/nar/gkt281

Yilmaz, A., M.Y. Nishiyama, B.G. Fuentes, G.M. Souza, D. Janies, J. Gray, et al. 2009. GRASSIUS: A platform for comparative regulatory genomics across the grasses. Plant Physiol. 149:171–180. doi:10.1104/pp.108.128579

Zhang, Y., I. von Behrens, R. Zimmermann, Y. Ludwig, S. Hey, and F. Hochholdinger. 2015. LATERAL ROOT PRIMORDIA 1 of maize acts as a transcriptional activator in auxin signalling downstream of the Aux/IAA gene *rootless with undetectable meristem 1*. J. Exp. Bot. doi:10.1093/jxb/erv187

Zhao, Q., J. Nakashima, F. Chen, Y. Yin, C. Fu, J. Yun, et al. 2013. Laccase is necessary and nonredundant with peroxidase for lignin polymerization during vascular development in Arabidopsis. The Plant Cell Online 25:3976–3987. doi:10.1105/tpc.113.117770

ZhiMing, Y., K. Bo, H. XiaoWei, L. ShaoLei, B. YouHuang, D. WoNa, et al. 2011. Root hair-specific expansins modulate root hair elongation in rice. Plant J. 66:725–734. doi:10.1111/j.1365-313X.2011.04533.x